Proceedings of the ASME 2009 28th International Conference on Ocean, Offshore and Arctic Engineering
OMAE2009
May 31 - June 5, 2009, Honolulu, Hawaii, USA

OMAE2009-79178

NONLINEAR SHIP MOTION COMPUTATIONS USING A TIME-DOMAIN BODY-EXACT SLENDER-BODY APPROACH

Piotr J. Bandyk*
Dept. of Naval Architecture & Marine Engineering
University of Michigan
Ann Arbor, Michigan 48109
Email: pbandyk@umich.edu

Robert F. Beck
Dept. of Naval Architecture & Marine Engineering
University of Michigan
Ann Arbor, Michigan 48109
Email: rbeck@umich.edu

ABSTRACT

This paper continues the development of a computationally efficient potential flow code using a time-domain body-exact strip theory approach. The exact body boundary conditions and linearized free surface conditions are used. Present results include further improvements, validations, and comparisons. Two different formulations to obtain the forces on the vessel are studied: pressure and momentum. Panel distribution techniques, critical for large amplitude motions, are discussed. The slender-body assumption requires finding the longitudinal interaction between sections to compute the hydrodynamic forces. Finally, an equation of motion solver is implemented to predict the six degree-of-freedom motions of the vessel in regular waves, including nonlinear effects.

INTRODUCTION

Nonlinear seakeeping methods have been under development and offer capabilities beyond classical linear strip theory. Fully nonlinear approaches have problems with numerical stability and wave breaking. So called blended methods have been used to fill the gap between the two ends of the spectrum. They can range in complexity and are often tailored for a particular problem. The objective of this paper is to discuss the development of a computationally efficient seakeeping code that has the ability to capture nonlinear forces acting on a ship.

The mixed Euler-Lagrange (MEL) method developed by Longuet-Higgins & Cokelet [1] has been used to solve nonlinear wave and wave-body interaction problems. The MEL approach can lead to numerical instabilities and wave breaking. Advanced numerical techniques can be used reduce some of these problems, but wave breaking is a natural occurrence and expected for large amplitude motions and waves. Methods dealing with this phenomenon numerically are generally not robust and may lead to nonphysical solutions. Moreover, solving the fully nonlinear water-wave problem is computationally expensive.

The body-exact approximation is a middle ground between the linear and fully nonlinear approaches. The mixed boundary value problem satisfies the linear free surface conditions and exact body boundary conditions on the instantaneous wetted surface. A time-domain approach allows for large amplitude motions including impact problems.

Zhang & Beck [2, 3] developed a two-dimensional body-exact method using desingularized sources above the free surface and constant strength panels to represent the body. A mathematically consistent three-dimensional approach was developed by Zhang [4], while the two-dimensional approach was expanded into a strip theory. Comparisons between the two methods were presented by Zhang et al. [5]. The results showed good agreement, although the strip theory showed advantages in computational speed and ease of modeling geometrically complex hull forms.

This paper presents the continuing development of a body-exact strip theory that was recently published by Bandyk & Beck [6]. This approach is applicable to slender monohulls. The boundary integral problem is split into two-dimensional transverse cuts, or strips, while taking into account the interaction between these strips. The result is a set of forces and moments acting on the vessel which can be used to solve the equations of motion in the case of a free running model. Specifically, this paper focuses on comparing two methods to compute the forces acting on the ship: pressure and momentum. The Euler equations

*Address all correspondence to this author.

of motion are used to compare vessel responses, including all six degrees of freedom.

MATHEMATICAL FORMULATION

Three coordinate systems are referenced: the $\mathbf{x_0}$ system is fixed in space, the $\mathbf{x}$ system is fixed to the mean position of the ship and translates at speed $\mathbf{U}(t)$ along the track of the ship, and the $\overline{\mathbf{x}}$ system is fixed to the ship. The origin of the $\mathbf{x}$ system is at the calm waterline at amidships. Consistent with a right-hand convention, the x-axis points in the direction of travel, the y-axis points to port on the calm water, and the z-axis points upward. The $\mathbf{x}$, or equilibrium, reference frame is used to solve the hydrodynamic problem, and therefore Bernoulli's equation is derived in this frame.

The fluid is assumed to be inviscid and incompressible. It is started from rest and remains irrotational. The effects of surface tension are neglected. This allows the use of a velocity potential, Φ, whose gradient gives the fluid velocities. The domain is bounded by the exact body surface, mean free surface, and surface at infinity. The total potential must satisfy Laplace's equation everywhere in the domain.

$$\nabla^2\Phi(x,y,z;t) = 0 \tag{1}$$

The total potential, Φ, can be written in terms of the free stream and perturbation potential, ϕ. The free stream potential is useful when the ship has a mean speed associated with it, such as constant forward speed. The perturbation velocity potential must satisfy Laplace's equation.

$$\Phi(x,y,z;t) = -U_o x + \phi(x,y,z;t) \tag{2}$$

$$\nabla^2\phi(x,y,z;t) = 0 \tag{3}$$

The boundary integral problem can be solved once the appropriate boundary conditions have been met. The total pressure is given by Bernoulli's equation

$$p = -\rho(\frac{\partial\phi}{\partial t} + \frac{1}{2}|\nabla\phi|^2 - U_o\frac{\partial\phi}{\partial x} + gz) \tag{4}$$

On the mean free surface, the linearized kinematic and dynamic free surface boundary conditions are used to march the free surface in time, ignoring downstream effects

$$\frac{\partial\zeta}{\partial t} = \frac{\partial\phi}{\partial z} \quad \text{on} \quad S_F \quad (z=0) \tag{5}$$

$$\frac{\partial\phi}{\partial t} = -g\zeta \quad \text{on} \quad S_F \quad (z=0) \tag{6}$$

where $z = \zeta(x,y,t)$ is the free surface elevation, g is the acceleration due to gravity, and S_F is the free surface. The velocity potential on the free surface must be known to solve the mixed boundary value problem.

Implementing the slender-body approximation, the three-dimentional velocity potential is reduced into a series of two-dimensional potentials. They must satisfy the two-dimensional Laplace equation on each transverse strip, and are subject to the free surface boundary conditions in Eqns. (5) and (6).

The hull surface can be defined by $y = \pm b(x,z)$. Three-dimensional unit normals to the body surface can be found as

$$\mathbf{n} = (n_1,n_2,n_3) = \frac{(\frac{\partial b}{\partial x}, \mp 1, \frac{\partial b}{\partial z})}{\sqrt{(\frac{\partial b}{\partial x})^2 + 1 + (\frac{\partial b}{\partial z})^2}} \tag{7}$$

where the normal direction points into the body.

Under the slender-body assumption, $\frac{\partial b}{\partial x} << (1, \frac{\partial b}{\partial z})$, and the strip theory unit normals are given by

$$\mathbf{N} = (N_1,N_2,N_3) = \frac{(\frac{\partial b}{\partial x}, \mp 1, \frac{\partial b}{\partial z})}{\sqrt{1 + (\frac{\partial b}{\partial z})^2}} \tag{8}$$

where the two-dimensional unit normal, $(0,N_2,N_3)$, has unity magnitude and is used to satisfy the two-dimensional body boundary conditions. It is useful to define (N_4,N_5,N_6) as

$$(N_4,N_5,N_6) = \mathbf{r} \times \mathbf{N} \tag{9}$$

where $\mathbf{r}$ is the position vector of the node, relative to the origin of the body axis system, in the body axis system.

Boundary Value Problem for ϕ

The perturbation potential on each section is broken up into four components

$$\phi(y,z;x,t) = \phi^i + \phi^d + \phi^r + \phi^a$$

where $\phi^i =$ incident wave potential
$\phi^d =$ diffracted potential
$\phi^r =$ radiated potential
$\phi^a =$ non-zero angle potential

The resulting exact body boundary conditions are re-written in two dimensions using the strip theory approach

$$\mathbf{N}\cdot\nabla\phi^d = -\mathbf{N}\cdot\nabla\phi^i \quad \text{on} \quad S_B \tag{10}$$

$$\mathbf{N}\cdot\nabla\phi^r = \mathbf{V}\cdot\mathbf{N} + \Omega\cdot(\mathbf{r}\times\mathbf{N}) \quad \text{on} \quad S_B \tag{11}$$

$$\mathbf{N}\cdot\nabla\phi^a = U_o(-\eta_6 N_2 + \eta_5 N_3) \quad \text{on} \quad S_B \tag{12}$$

where $\mathbf{V}$ and Ω are the translational and rotational velocities of the body. η_i represents the three translations ($i = 1,2,3$) and rotations ($i = 4,5,6$) of the body-fixed frame $\overline{\mathbf{x}}$ relative to the equilibrium frame $\mathbf{x}$ with respect to the x-, y-, and z-axes. The terms

on the right hand side of Eqns. (10) and (11) represent the instantaneous velocity of the fluid in order to satisfy the corresponding body boundary conditions. The terms on the right hand side of Eqn. (12) are the two-dimensional corrections when there is a non-zero pitch angle, η_5, or non-zero yaw angle, η_6, in the case of forward speed. This correction assumes small angles relative to the equilibrium frame, such that $sin(\eta_{5,6}) \approx \eta_{5,6}$.

The velocity potential is known on the mean free surface. In the far field, a radiation boundary condition is imposed such that only the incident waves are incoming. This is done numerically by incorporating an outer "beach" region, with exponentially increasing node spacing, which absorbs outgoing waves. Also, the water is assumed deep and the gradient of the perturbation potential vanishes as $z \rightarrow -\infty$. The incident wave potential is known, while the other potentials must be computed. They are initially set to zero and the dynamics (ship motions or incident wave elevation) are ramped using a hyperbolic tangent function.

Once the mixed boundary value problem is solved, the velocity potential and its derivatives can be determined anywhere in the fluid domain. The pressure on the body can be determined by using Bernoulli's equation (4). The free surface conditions are time-stepped using Eqns. (5) and (6).

Momentum Formulation

The momentum formulation requires solving the ϕ problem first. However, the resulting formulae do not calculate the pressure on the body to find the forces and moments. This was derived as an alternative to the direct pressure integration for the "swimming fish" problem by Newman and Wu [7]. The derivation, including a free surface, is shown in Sclavounos [8]. The main difference is the use of the $z = 0$ for the free surface conditions, instead of the weak scatterer assumption by Sclavounos. The result is the following approximation for the dynamic sectional forces

$$\mathbf{f}_d \approx -\rho \int_{S_B} p\mathbf{N} dl \tag{13}$$

$$\mathbf{f}_d \approx -\rho \frac{d}{dt} \int_{S_B} \Phi \mathbf{N} dl - \rho \int_{S_{WP}} (g\zeta^i + \frac{d\phi^i}{dt})\mathbf{N} dl \tag{14}$$

where S_{WP} is the exact waterplane surface intersecting the body.

The total dynamic forces and moments can be written in terms of the perturbation potential

$$\mathbf{F}_d \approx -\rho \int_L dx [\frac{\partial}{\partial t} \int_{S_B} \phi \mathbf{N} dl - U_o \frac{\partial}{\partial x} \int_{S_B} \phi \mathbf{N} dl + \int_{S_{WP}} (g\zeta^i + \frac{d\phi^i}{dt})\mathbf{N} dl] \tag{15}$$

The speed dependent component of the force is apparent in the second term. Numerically, this is much simpler than approximating $\frac{\partial \phi}{\partial x}$ at every node. A drawback of the momentum approach is that the pressure distribution is not known.

Boundary Value Problem for $\frac{\partial \phi}{\partial t}$

Eqn. (4) requires a knowledge of $\frac{\partial \phi}{\partial t}$ to find the pressure on the body. Using numerical differentiation to find this term may lead to problems for large amplitude motions. An alternative method is to solve for the $\frac{\partial \phi}{\partial t}$ term directly. An auxiliary mixed boundary value problem is set up to solve for $\psi = \frac{\delta \phi}{\delta t}$, the time derivative following a moving node. It can be related to the partial time derivative by $\frac{\partial \phi}{\partial t} = \psi - \mathbf{v} \cdot \nabla \phi$, where $\mathbf{v}$ is the node velocity in the equilibrium frame.

The mixed boundary value problem requires ψ on the free surface and $\mathbf{N} \cdot \nabla \psi$ on the body. The free surface conditions are already known from Eqn. (6). The body boundary conditions require taking the appropriate time-derivatives of Eqns. (10) through (12). The resulting boundary conditions can be found after a bit of vector calculus

$$\mathbf{N} \cdot \nabla \psi^d = -\mathbf{N} \cdot \nabla \psi^i + \frac{\delta \mathbf{N}}{\delta t} \cdot (-\nabla \phi^d - \nabla \phi^i) \quad \text{on} \quad S_B \tag{16}$$

$$\mathbf{N} \cdot \nabla \psi^r = \mathbf{a} \cdot \mathbf{N} + \frac{\delta \mathbf{N}}{\delta t} \cdot (-\nabla \phi^r + \mathbf{v}) \quad \text{on} \quad S_B \tag{17}$$

$$\mathbf{N} \cdot \nabla \psi^a = \frac{\delta \mathbf{N}}{\delta t} \cdot (-\nabla \phi^a + U_o \mathbf{i}) \quad \text{on} \quad S_B \tag{18}$$

where $\mathbf{a}$ and $\mathbf{v}$ are the body acceleration and velocity in the body axis system, respectively, including rotational terms. It should be noted that Eqns. (16) through (18) are solved in the equilibrium axis system. The scalar quantities are, of course, independent of axis system choice. For ease of computation, the vector and gradients on the right hand side are evaluated in the body axis system. In order to determine $\frac{\delta \mathbf{N}}{\delta t}$ in the equilibrium frame, the following identity is used

$$(\frac{\delta \mathbf{N}}{\delta t})_{equilibrium} = (\frac{\delta \mathbf{N}}{\delta t})_{body} + \Omega \times \mathbf{N} \tag{19}$$

where the first term on the right hand side is zero, by definition.

It is worth noting that the acceleration term in Eqn. (17) requires special treatment in the case of free motions. The terms can be resolved into a six-by-six matrix, for each degree of freedom, and moved to the other side of the equations of motion. A canonical problem is set up which solves $\psi_i = 0$ on the free surface, $\mathbf{N} \cdot \nabla \psi_i = N_i$ on the body, for $i = 1..6$, and a final problem including the memory effects of the perturbed wave field. The derivation of a similar approach in an unbounded fluid can be found in Chapter 4 of Newman [9].

NUMERICAL METHODS

At each time step a mixed boundary value problem must be solved; ϕ is given on the free surface and its normal derivative is known on the body surface. The free surface boundary conditions are determined from the time marching of Eqns. (5) and (6), while the body boundary conditions are given by prescribed motions or an equations of motion solver. Desingular-

ized sources are placed above the linearized free surface and constant strength panels are used to model the instantaneous wetted body geometry, up to the incident wave elevation. The mixed boundary value problem is solved by Gaussian elimination and the source strengths are determined. At this point, ϕ and its gradient are known everywhere in the domain. The x-derivative of the velocity potential must be estimated using numerical techniques. Using this approach to find derivatives of known functions is discussed by Buhmann [10]. Details on how this is applied to the current method can be found in Zhang et al. [5]. The pressure or momentum formulation may be followed to determine the forces on the hull. The momentum formulation is presented in the previous section.

The improved pressure formulation requires solving the ψ problem, as discussed in the previous section. An advantage of this method is that it is not sensitive to the time-step size when computing the pressure on the body, since $\frac{\partial \phi}{\partial t}$ is solved for directly. Another advantage is that this method is robust for large amplitude motions and indifferent to panel variations between time-steps. Once the pressure is found everywhere on the body, the forces acting on the body can be approximated by integrating Eqn. (4) over the instantaneous submerged body surface. Under the slender-body assumption, they are

$$\mathbf{F} \approx \int_L dx \int_{S_B} p\mathbf{N}\, dl \tag{20}$$

$$\mathbf{M} \approx \int_L dx \int_{S_B} p(\mathbf{r} \times \mathbf{N})\, dl \tag{21}$$

where $\mathbf{F}$ are the three forces and $\mathbf{M}$ are the three moments acting on the vessel.

Once the forces and moments are known, the equations of motion can be solved. The Euler equations of motion (see Fossen [11] for details) are solved and the body velocity and position vectors are updated using a fourth-order Adams-Bashforth time-stepping method. The roll moment includes an empirical viscous roll damping model developed by Himeno [12]. A fourth-order Adams-Bashforth method is also used to time-step the free surface conditions.

As the vessel translates and rotates relative to the equilibrium frame, translating at U_o, the body must be re-panelized. A "fixed panel" technique is used to model the instantaneous wetted geometry. The maximum number of panels is determined at the start of the simulation and models the entire hull, up to the sheer line and closed off with a flat deck. The number of "wet" panels is determined by the intersection of the body and the incident wave. The number of panels can change in between time steps, as numerical problems associated with this are avoided when using either the improved pressure or momentum formulation. Special care must be taken where the panel intersects the incident free surface. Panels are truncated at the free surface and, if they are relatively small enough, may be combined with an adjacent panel. This is done to ensure reasonable influence matrix condition numbers. When a section exits the water, computations are simply stopped. Upon re-entry, they are restarted with initial conditions of zero for that particular section.

RESULTS AND DISCUSSION

Convergence studies have been carried out but will not be presented here, due to the limited availability of space. They can be found in Zhang [4] for the two-dimensional problems. Zhang et al. [13] discuss more detailed convergence studies including the current body-exact strip theory. A range of validations can be found in Bandyk and Beck [6]. A variety of results and comparisons are presented in this paper, including: the improved panelization technique implemented in this code; numerical and direct solution of the $\frac{\partial \phi}{\partial t}$ term in the pressure equation for small and large amplitude motions; pressure and momentum formulation results for six degree-of-freedom small amplitude motions. In this paper, all the computations are done using the S-175 containership. The length, beam, and draft of the vessel are 175.0, 25.4, and 9.5 meters, respectively. The vessel has a block coefficient of 0.571 and waterplane coefficient of 0.711.

Direct Solution of ψ

Forced heave simulations are used to validate the ψ formulation. The dynamic heave forces on a typical midship section will be shown and discuss for a variety of amplitudes. The dynamic force components include the radiation memory and impulsive components. The impulsive component is the solution of the radiation problem with $\phi = 0$ on the free surface, while the memory term accounts for the free surface radiation disturbance.

The first test case is for small amplitude forced heave, where the panel number doesn't change. Figure 1 shows a comparison between the numerical differentiation to estimate $\frac{\partial \phi}{\partial t}$ using $\Delta t = T/50, T/100, T/200$ and the direct solution using $\Delta t = T/50$, where T is the period of oscillation and Δt is the time-step size. The memory component is the upper set of curves, in blue, and the impulsive components is the lower set, in red. This simple case confirms that the direct solution (solid lines), at a course time-step size, yields a result that the numerical differentiation approaches as the time-step becomes smaller (increasingly lighter dashed lines). A zoomed view of this convergence can be seen in Figure 2. The advantages are already apparent: a more course time-step can be used in exchange for a few more back substitutions with the inverted influence matrix.

The fixed panelization offers many advantages over a "rubber banding" method; no need to repanelize and recompute normals, and the ability to easily capture hard corners like chines. Unfortunately, fixed panelization has problems when adding and removing panels. However, the improved pressure formulation, solving the ψ problem, resolves this complication. Figure 3 shows a small amplitude where just one panel is added or removed, in comparison to the previous results. The spikes can be seen in the cases of numerical differentiation (dashed lines) around 16 and 21 seconds in both force components. The two instances of time correspond to adding or removing one panel on either side of a symmetric section in this case of forced heave

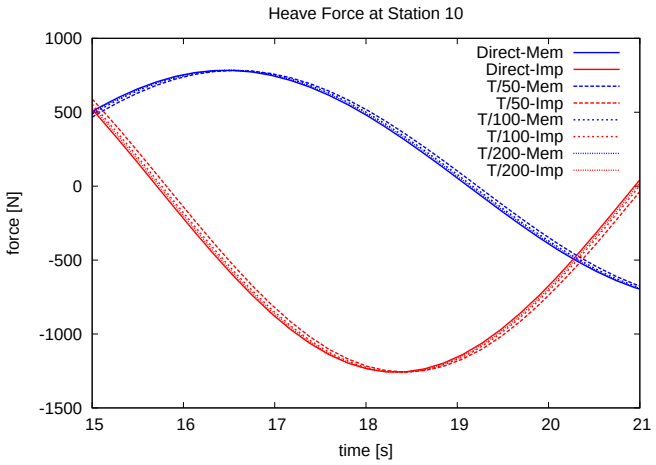

Figure 1. SECTIONAL HEAVE FORCE, AMPLITUDE = 0.01m

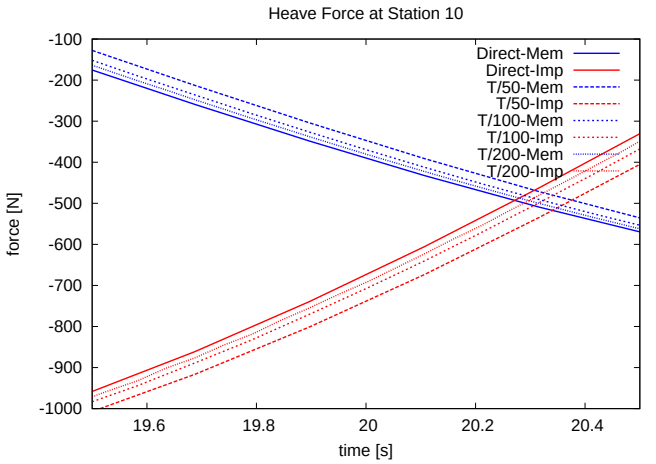

Figure 2. ZOOM: SECTIONAL HEAVE FORCE, AMPLITUDE = 0.01m

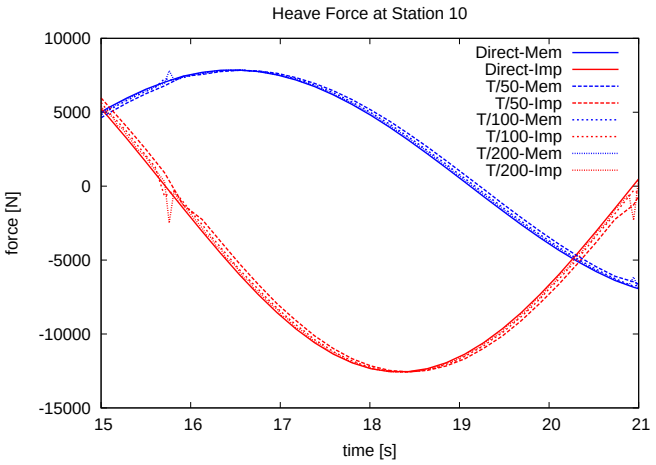

Figure 3. SECTIONAL HEAVE FORCE, AMPLITUDE = 0.10m

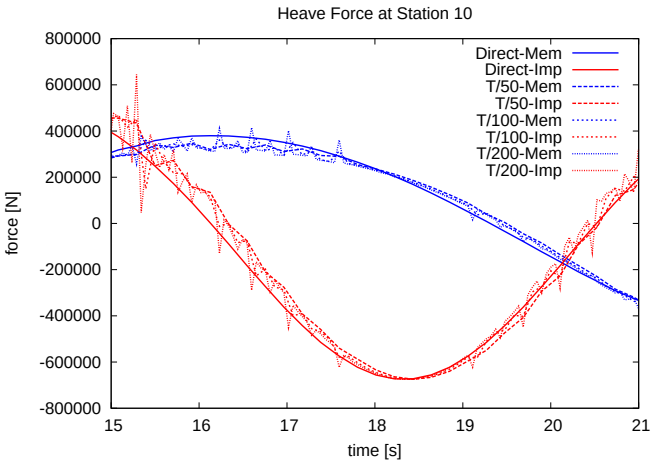

Figure 4. SECTIONAL HEAVE FORCE, AMPLITUDE = 5.00m

periodic motions. The spikes actually increase as the time-step is reduced.

However, the direct solution does not show this sensitivity to different panelization between time-steps. Moreover, for prescribed motions, only the evolution of the free surface conditions is sensitive to time-step size. Since they are linearized as shown in Eqns. (5) and (6), a more course time-step can be used which offers significant savings in computational effort.

As an extreme example, a large amplitude case is also done. The heave amplitude is about half of the draft. In this case, many panels are added and removed as the vessel motions are very significant. Figure 4 shows the how much smoother the force time-series is when solving the ψ problem directly.

More complicated sections show even more drastic differences between the direct and approximate solutions for large amplitude cases. This simple section was used to illustrate the already visible advantages of using the direct solution with fixed panelization.

Six Degree-of-Freedom Euler Equations

This section presents response amplitude operator (RAO) results for the S-175 at $Fn = 0.0, 0.2$ in all six degrees-of-freedom, as shown in Figures 5 through 28. It is worth noting that the extensive free motion results have been checked for convergence in temporal and spatial resolution. All the cases are long crested regular waves with amplitude of $0.1m$. A range of 5 heading angles are considered, $\beta = 0$, 45, 90, 135, and 180 degrees where $\beta = 180$ degrees is head seas. The small amplitude wave is used for two reasons: to minimize the amount of drifting off-course from second-order forces; and to compare to a linear code. The code used for comparison is SHIMPO, a strip theory based on the work presented in Beck [14].

In the body-exact formulation, the ship would not remain course steady due to higher-order physical drift forces and slight numerical inaccuracies. This is especially evident with increasing forward speed. The horizontal plane modes of motion have no restoring mechanisms so any perturbation will propogate. Therefore, the surge, sway, and yaw motions have light forcing

added in the transient ramp-up to minimize this drift. This is the simplest way to slightly control the free motions so that they can be compared to linear results. This artificial force is decreases as the transients die off, thus negligibly affecting the dynamics of small amplitude motions. The body-exact time-domain formulation will require a controller to prevent the vessel from drifting off-course in the cases of large amplitude free motions.

Simulations were executed using both the pressure and momentum formulations. They are nearly identical in the zero speed case, as expected. There are some differences in the forward speed results. This is due to the treatment of the $\frac{\partial}{\partial x}$ terms. Overall, there is good agreement between the two methods and SHIPMO. Neither method is superior when it comes to the forward speed cases. In certain cases, like surge motions for beam seas in Figure 17, it appears that one method compares better than the other. However, the scale of the RAO results must be taken into consideration and the motions are negligible. In certain cases the heave-pitch coupling is significant with forward speed, and we see worse agreement with SHIPMO. For example, the heave and pitch motions in Figures 9 and 10 or Figures 25 and 27 show significant heave and pitch motions at forward speed around $L/\lambda = 0.9$ or 1.0, respectively. The yaw responses in quartering seas, Figures 16 and 28, show an over-estimate of the forward speed effects, relative to the zero speed results, when compared to SHIPMO. The differences in these forward speed results are currently being investigated.

CONCLUSIONS

The results shown are very encouraging. The small amplitude free motions compare very well with linear theory in all six degrees-of-freedom. This is a meaningful realization, as classical linear strip theory is based in the frequency domain and fully linearized. No drift is present and the body does not have to be repanelized. The capabilities of the time-domain body-exact code exceed those of a fully linear code, although it should reduce to the linear code for small amplitudes. The good comparison for this small amplitude motion validates this time-domain code against the arguments made by linear theory.

The combination of fixed panelization and direct solution of $\frac{\partial \phi}{\partial t}$ proves to be the most robust and accurate method when computing the pressure on the hull. The hull is modeled more accurately, repanelization is more straightforward than "rubber banding", matrix condition numbers remain reasonable, and calculating the pressure on the body is no longer dependent on the time step. The numerical approximation of $\frac{\partial \phi}{\partial x}$ seems to work well, but may still be improved upon.

The final steps in this research are to add a controller and allow the vessel to follow a prescribed path, including yaw. The result will be a coupled model of nonlinear seakeeping and maneuvering that is computationally efficient. The results shown can be computed close to "real-time" on a more powerful desktop computer. The method could be used as a design tool or for path optimization.

ACKNOWLEDGMENT

This work was supported by the Office of Naval Research, contracts N00167-04-D-0004, N00014-05-1-0537, and N00014-06-1-0879.

REFERENCES

[1] Longuet-Higgins, M. S., and Cokelet, E. D., 1976. "The deformation of steep surface waves on water. i. a numerical method of computation". In Royal Society of London. Series A: Mathematical and Physical Sciences, Vol. 350, pp. 1–26.

[2] Zhang, X. S., and Beck, R. F., 2006. "2-d body-exact computations in the time domain". In 21st International Workshop on Water Waves and Floating Bodies, pp. 197–200.

[3] Zhang, X. S., and Beck, R. F., 2007. "Computations for large-amplitude two-dimensional body motions". *Journal of Engineering Mathematics (Special Volume in Honor of J. N. Newman)*.

[4] Zhang, X. S., 2007. "Large amplitude ship motion computations using a time dependent body geometry". Phd thesis, The University of Michigan, Department of Naval Architecture and Marine Engineering.

[5] Zhang, X. S., Bandyk, P. J., and Beck, R. F., 2007. "Large amplitude body motion computations in the time-domain". In 9th International Conference on Numerical Ship Hydrodynamics.

[6] Bandyk, P. J., and Beck, R. F., 2008. "Nonlinear ship motions in the time-domain using a body-exact strip theory". In 27th Int'l Conference on Offshore Mechanics and Arctic Engineering, ASME.

[7] Newman, J. N., and Wu, T. Y., 1973. "A generalized slender-body theory for fish-like forms". *Journal of Fluid Mechanics Digital Archive*, **57**(04), pp. 673–693.

[8] Sclavounos, P. D., 2008. Nonlinear response modeling of a vessel in steep random waves. Personal Correspondence with R. F. Beck.

[9] Newman, J. N., 1977. *Marine Hydrodynamics*. MIT Press.

[10] Buhmann, M. D., 2000. "Radial basis functions". *Acta Numerica*, pp. 1–38.

[11] Fossen, T. I., 1994. "Modeling of marine vehicles". In *Guidance and Control of Ocean Vehicles*. John Wiley and Sons, ch. 2, pp. 5–56.

[12] Himeno, Y., 1981. Prediction of ship roll damping-state of the art. Tech. Rep. 239, University of Michigan, Dept. of Naval Architecture and Marine Engineering.

[13] Zhang, X. S., Bandyk, P. J., and Beck, R. F., 2008. "Time-domain simulations of radiation and diffraction forces". *Submitted to the Journal of Ship Research*.

[14] Beck, R. F., 1989. "Ship responses to regular waves". In *Principles of Naval Architecture*, Vol. III. SNAME, ch. 8, pp. 41–83.

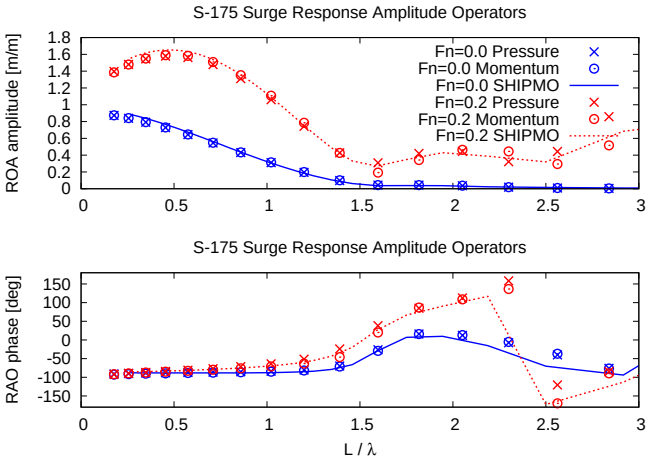

Figure 5. S-175 SURGE RAO IN FOLLOWING SEAS

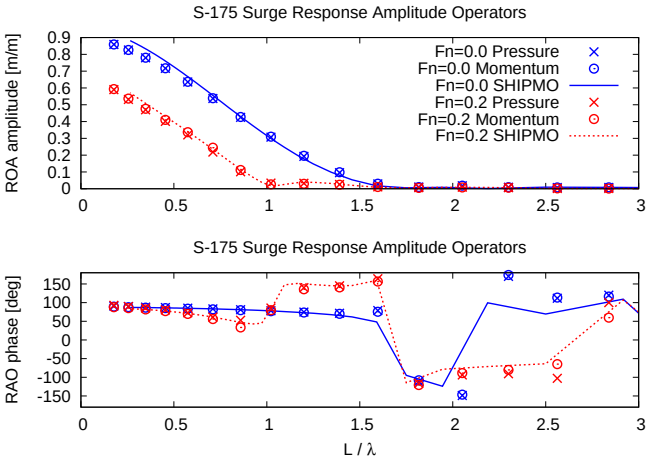

Figure 8. S-175 SURGE RAO IN HEAD SEAS

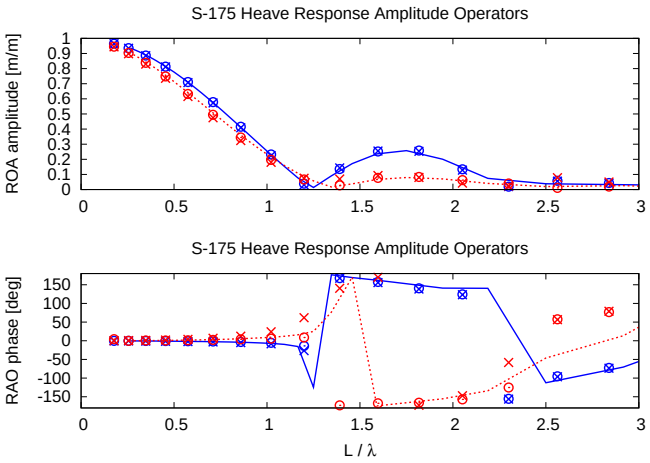

Figure 6. S-175 HEAVE RAO IN FOLLOWING SEAS

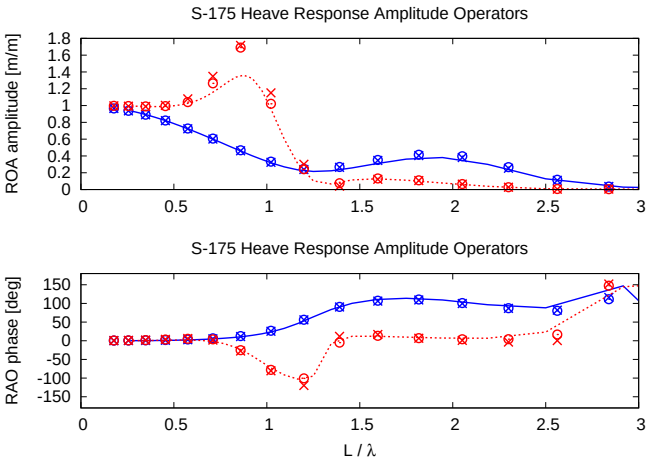

Figure 9. S-175 HEAVE RAO IN HEAD SEAS

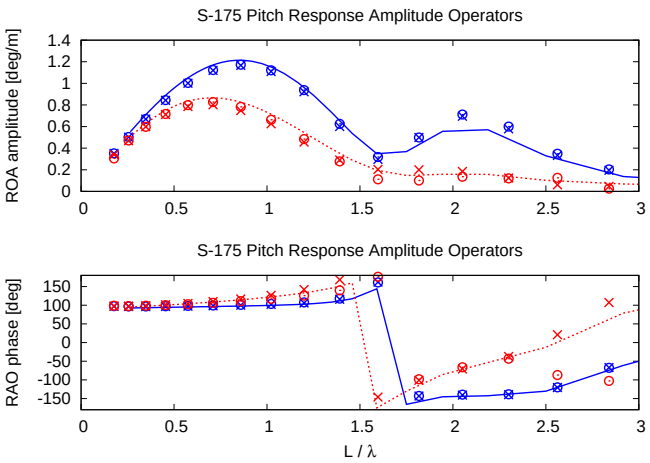

Figure 7. S-175 PITCH RAO IN FOLLOWING SEAS

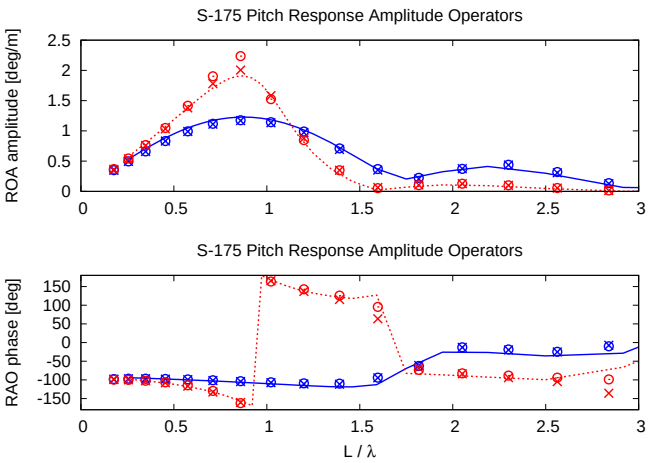

Figure 10. S-175 PITCH RAO IN HEAD SEAS

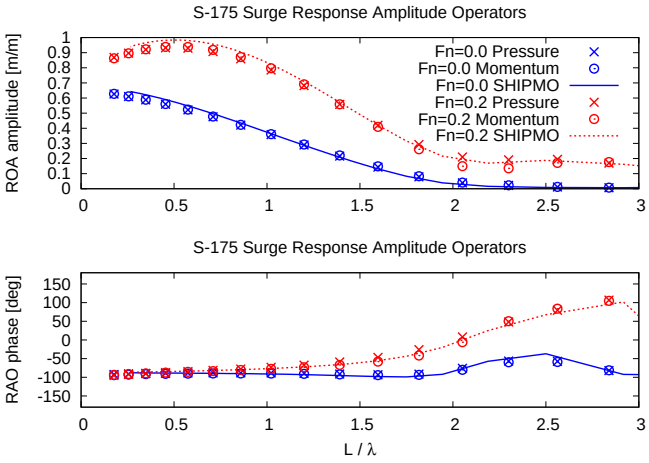

Figure 11. S-175 SURGE RAO IN STERN QUARTERING SEAS

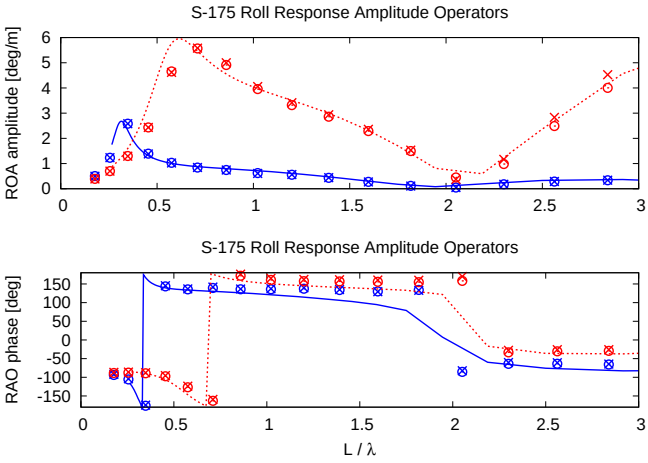

Figure 14. S-175 ROLL RAO IN STERN QUARTERING SEAS

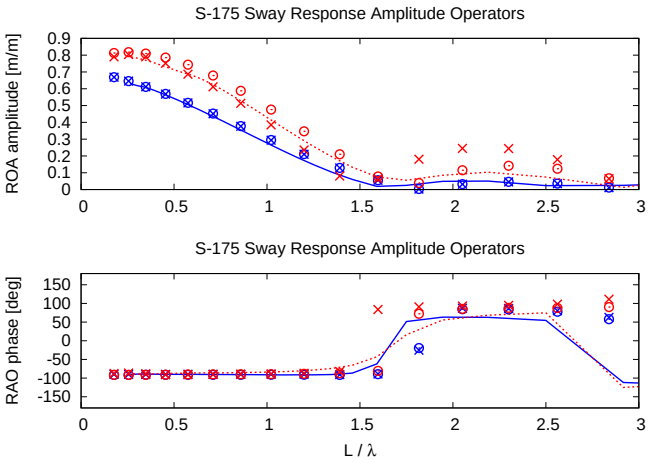

Figure 12. S-175 SWAY RAO IN STERN QUARTERING SEAS

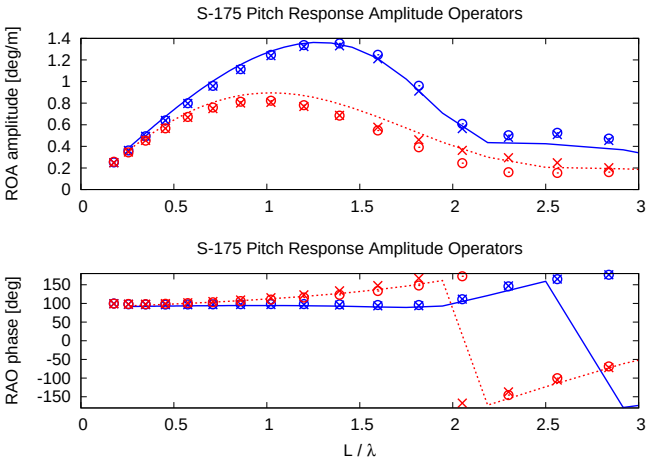

Figure 15. S-175 PITCH RAO IN STERN QUARTERING SEAS

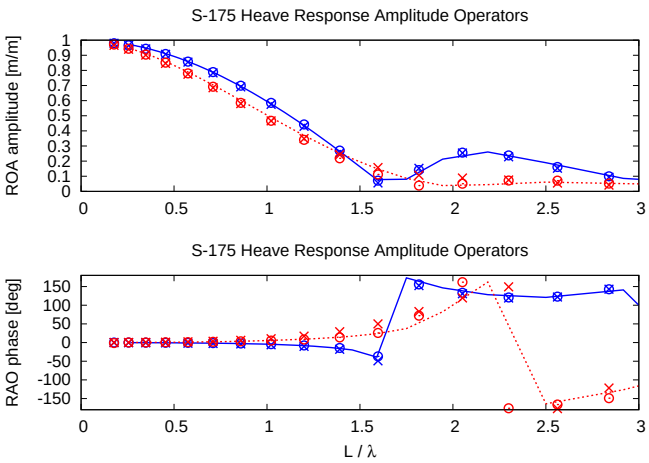

Figure 13. S-175 HEAVE RAO IN STERN QUARTERING SEAS

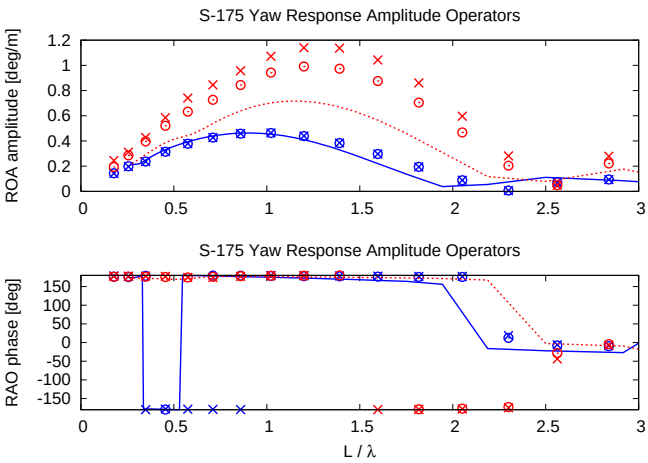

Figure 16. S-175 YAW RAO IN STERN QUARTERING SEAS

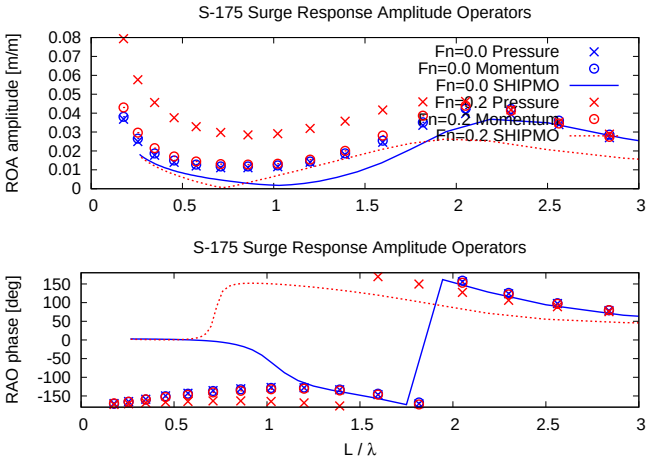

Figure 17. S-175 SURGE RAO IN BEAM SEAS

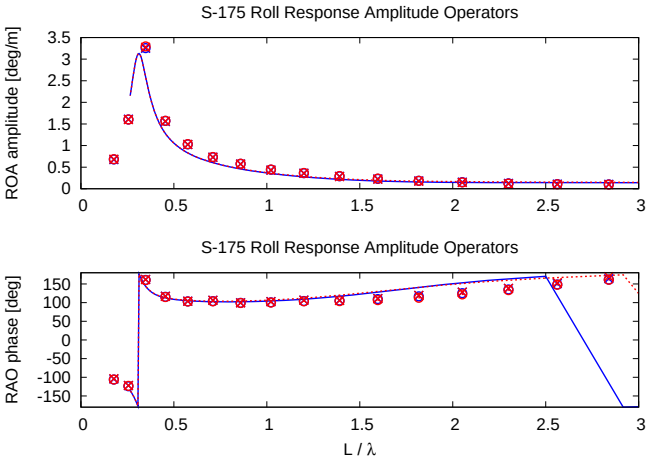

Figure 20. S-175 ROLL RAO IN BEAM SEAS

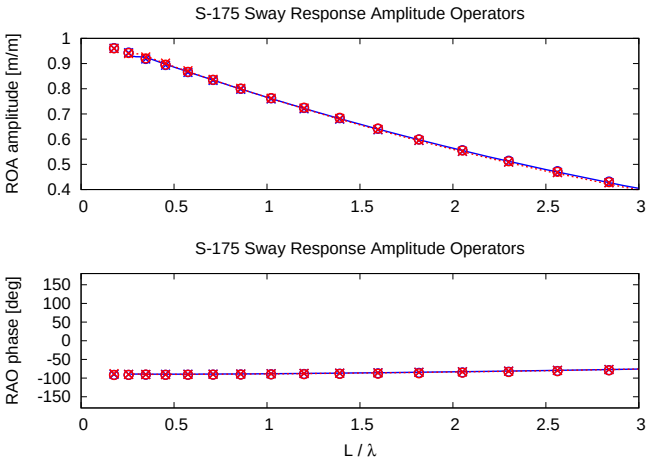

Figure 18. S-175 SWAY RAO IN BEAM SEAS

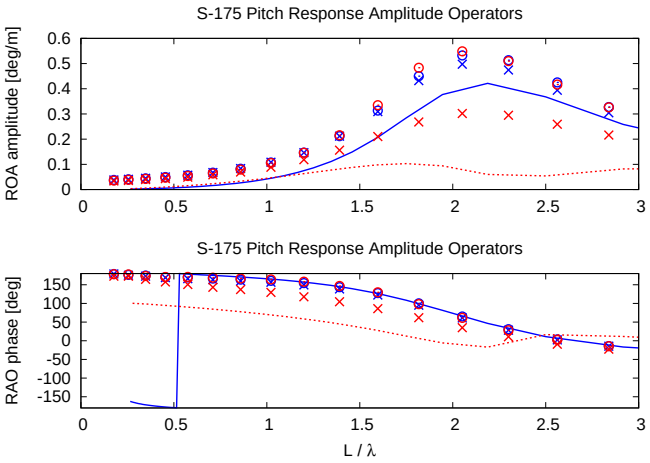

Figure 21. S-175 PITCH RAO IN BEAM SEAS

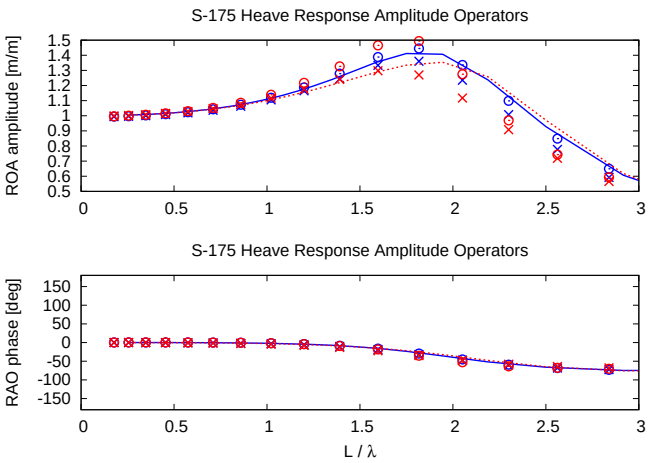

Figure 19. S-175 HEAVE RAO IN BEAM SEAS

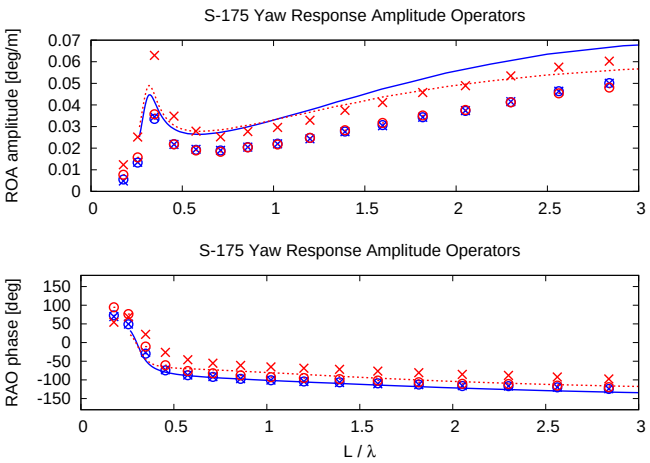

Figure 22. S-175 YAW RAO IN BEAM SEAS

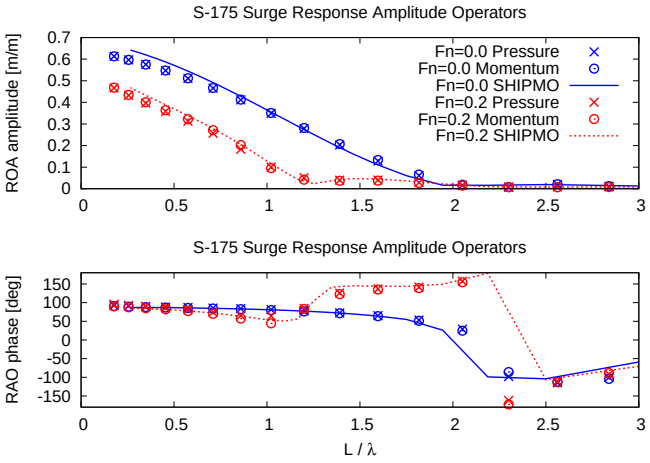

Figure 23. S-175 SURGE RAO IN BOW QUARTERING SEAS

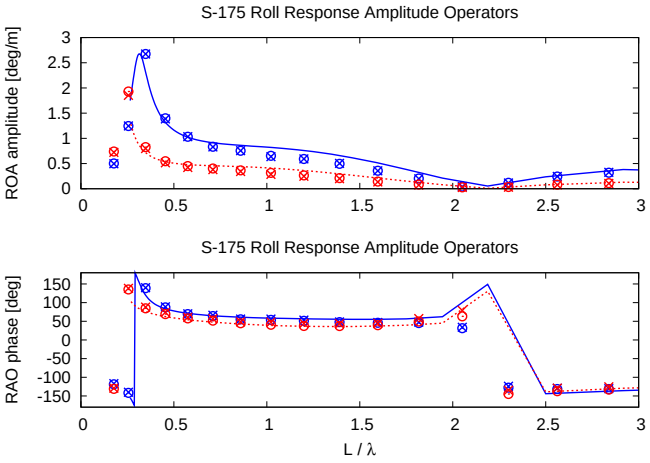

Figure 26. S-175 ROLL RAO IN BOW QUARTERING SEAS

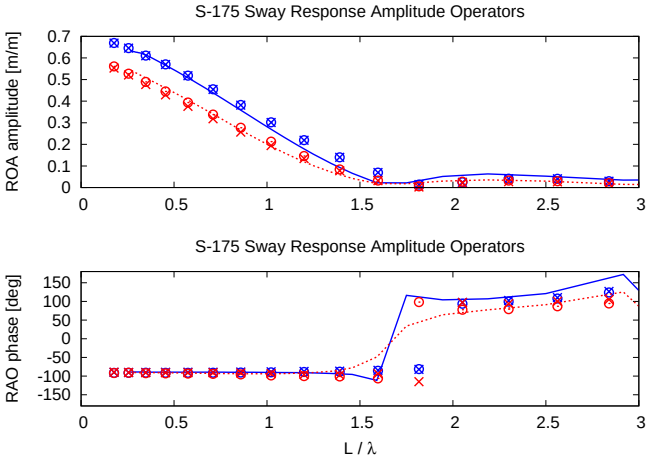

Figure 24. S-175 SWAY RAO IN BOW QUARTERING SEAS

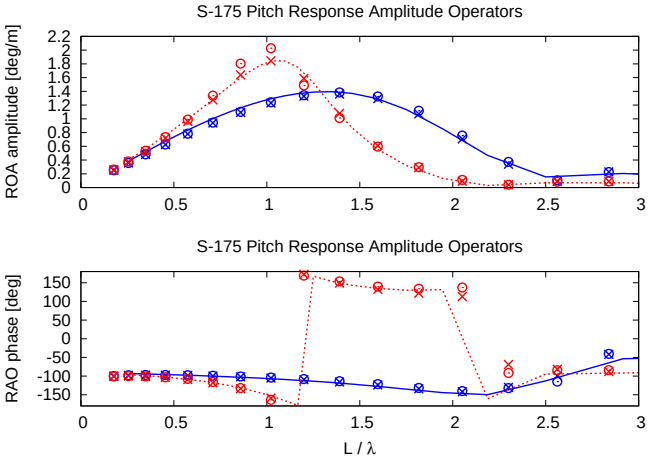

Figure 27. S-175 PITCH RAO IN BOW QUARTERING SEAS

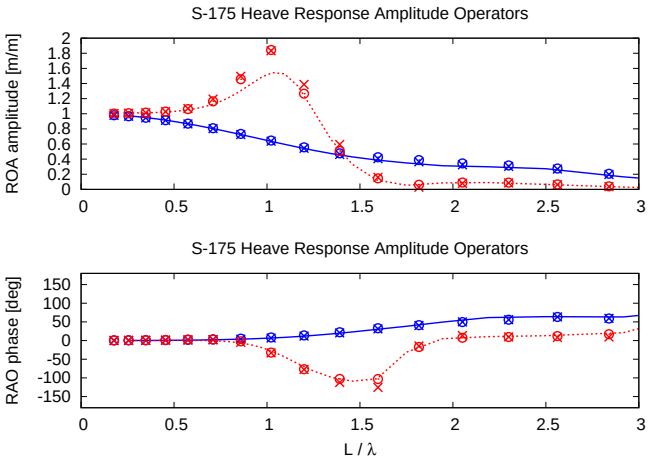

Figure 25. S-175 HEAVE RAO IN BOW QUARTERING SEAS

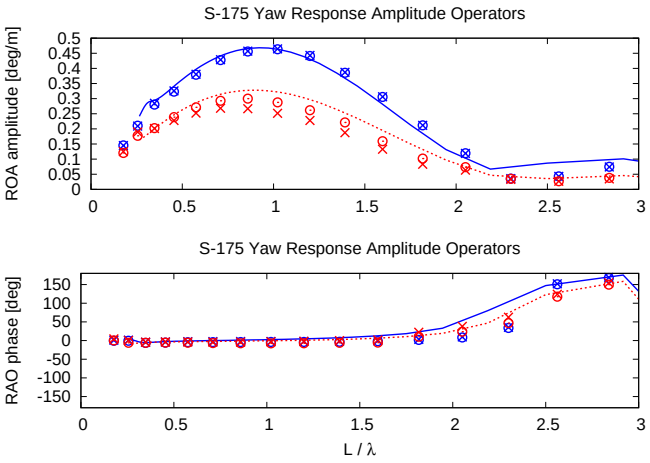

Figure 28. S-175 YAW RAO IN BOW QUARTERING SEAS